Atomic defects in monolayer ordered double transition metals carbide ($Mo_2TiC_2T_x$) MXene and CO_2 Activation

Rasoul Khaledialidusti,*[a] Abhishek Kumar Mishra,[b] Afrooz Barnoush[a,c]

[a]Department of Mechanical and Industrial Engineering, Norwegian University of Science and Technology (NTNU), 7491 Trondheim, Norway. E-mail: rasoul.khaledialidusti@ntnu.no

[b]Department of Physics, School of Engineering, University of Petroleum and Energy Studies, Bidholi via Premnagar, Dehradun 248007, INDIA.

[c]Curtin Corrosion Centre, WASM-MECE, Curtin University, Australia.

Transition metal carbides (MXenes) with formulas $M_{n+1}C_nT_x$ (n = 2 and 3) are emerging as a new family of two-dimensional (2D) materials providing great potential in electronic applications and CO_2 conversion catalysts. It has been found already that the electronic and electrochemical properties of $Ti_3C_2T_x$ MXenes can be tuned by replacing the two outer titanium layers with molybdenum layers. Similar to other 2D materials, intrinsic defects form in MXene flakes during the etching and delamination and the formation of defects in MXenes can influence the performance of these materials. Herein, we systematically study the effect of the different types of structural defects on the structural stability, electronic behavior, and electrochemical properties of ordered $Mo_2TiC_2T_x$ terminated with specific surface functions of fluorine, oxygen or hydroxide. The calculated defect formation energies imply that the formation of defects is dependent on the surface terminations, where the O-terminated MXenes demand more energy than F- and OH-terminated MXenes. We found that the defect formation is more feasible in outer molybdenum layers than the inner titanium layer. Our results predicted that the CO_2 molecule adsorbs on the defected surfaces through a spontaneous and exothermic process that is critical to its activation, while the perfect surface weakly attracts the molecule through a nonspontaneous and endothermic process. Thus, our study predicts that the electronic and electrochemical properties of $Mo_2TiC_2T_x$ can be tuned by forming the specific defects and these Mxenes can be promising materials for CO_2 activation and conversion.

1 Introduction

MXene are 2D materials that have shown great promise in energy storage applications,[1] including lithium-ion batteries,[2,3] supercapacitors,[4] and catalysis.[5] Quasi-two-dimensional (2D) $Mo_2TiC_2T_x$ is a an ordered double transition metals MXene, synthesized in 2015[6], in which the outer titanium layers in

$Ti_3C_2T_x$ (the first MXene discovered in 2011[7]) are replaced with molybdenum layers. In this MXene, the titanium layer is sandwiched by the molybdenum layers and carbon atoms occupy the octahedral sites between these two transition metals, as shown in **Fig. 1a**. It was exhibited that the electrochemical and electronic properties of the ordered $Mo_2TiC_2T_x$ MXene are different from $Ti_3C_2T_x$ MXene.[6,8] While $Ti_3C_2T_x$ is a metallic-like conductor,[6,9] it was confirmed that $Mo_2TiC_2T_x$ exhibits semiconductor-like transport behavior.[6,8] It was predicted that the ordered $Mo_2TiC_2T_x$ MXene terminated by the F group would be more semiconductor than that of terminated by OH group, while -O termination would provide a metallic behavior.[8]

Defects in 2D materials have a great impact on their properties, such as mechanical, electrical, optical, thermal, and magnetic properties. Similar to other 2D materials, the presence of intrinsic defects might alter the electronic and electrochemical properties of monolayer $Mo_2TiC_2T_x$ MXene. Intrinsic defects such as atomic vacancies and vacancy clusters were observed using scanning tunneling microscopy (STM) images in synthesized MXene flakes.[10,11] Etching and delamination conditions might affect the defect concentrations of MXene flakes that lower defect concentrations were observed at milder etching and delamination conditions.[10,12,13] Therefore, the formation of different kinds of defects is unavoidable in MXenes. Defect formations were also observed in other 2D materials, such as graphene,[14–16] BN,[17–19] and MoS_2.[20,21] It has been well documented that the presence of defects affect the electrical, electrochemical, electronic, optoelectronic, and mechanical properties of these 2D materials.[14–16,18,20]

Structural defects in 2D materials could be unfavorable. For example, the presence of defects leads to weakening the mechanical strength[15,22] and the electronic performance of graphene.[23] However, certain types of defects could be favorable and provide applicable functionalities by adjusting the local properties. For example, the mechanical properties of graphene could be increased by controlled defect creation[15] or the properties of MoS_2 could be tailored by controlled defect formation.[20] Compared to these 2D materials, while intrinsic defects were previously observed in MXene flakes,[10,11] the influence of defects on the electronic and electrochemical properties of MXenes has not extensively been investigated. From the rare investigations,[10,24,25] it was confirmed that the defects have unfamiliar effects on the MXene properties comparing to other 2D materials depending on the type of the defects,

reconstruction of the structure, and local chemical bonding.[10,24,25] It was predicted that titanium vacancies in $Ti_3C_2T_x$ MXene could not alter the metallic conductivity considerably; however, they affect surface morphology and terminations.[10] The effects of carbon vacancies in Ti_2CT_x indicated the improvement of electronic conductivity and the enhancement of mechanical flexibility.[24] It was also investigated that the intrinsic defects in Ti_2XT_x (X = C, N) MXenes could change the electronic properties from metallic to semiconducting or from semiconducting to metallic depending on the type of the defects and the system.[25]

Previous works indicate that various MXenes with different transition metals and functional groups might exhibit quite different behavior toward defects because of the comparatively complex structures and variety of chemical bonding between atoms. Despite tuning the electronic and electrochemical properties of $Ti_3C_2T_x$ MXene by manipulating the outer transition metal layers,[6] which are important for electronics, energy storage, sensing, and other applications, the presence of defects might significantly change the properties of ordered $Mo_2TiC_2T_x$ MXene. Therefore, a detailed atomistic understanding of the influence of the different types of defects on the electronic and electrochemical properties of ordered $Mo_2TiC_2T_x$ MXene is important to explore its real-device applications, in which understanding these properties are crucial.

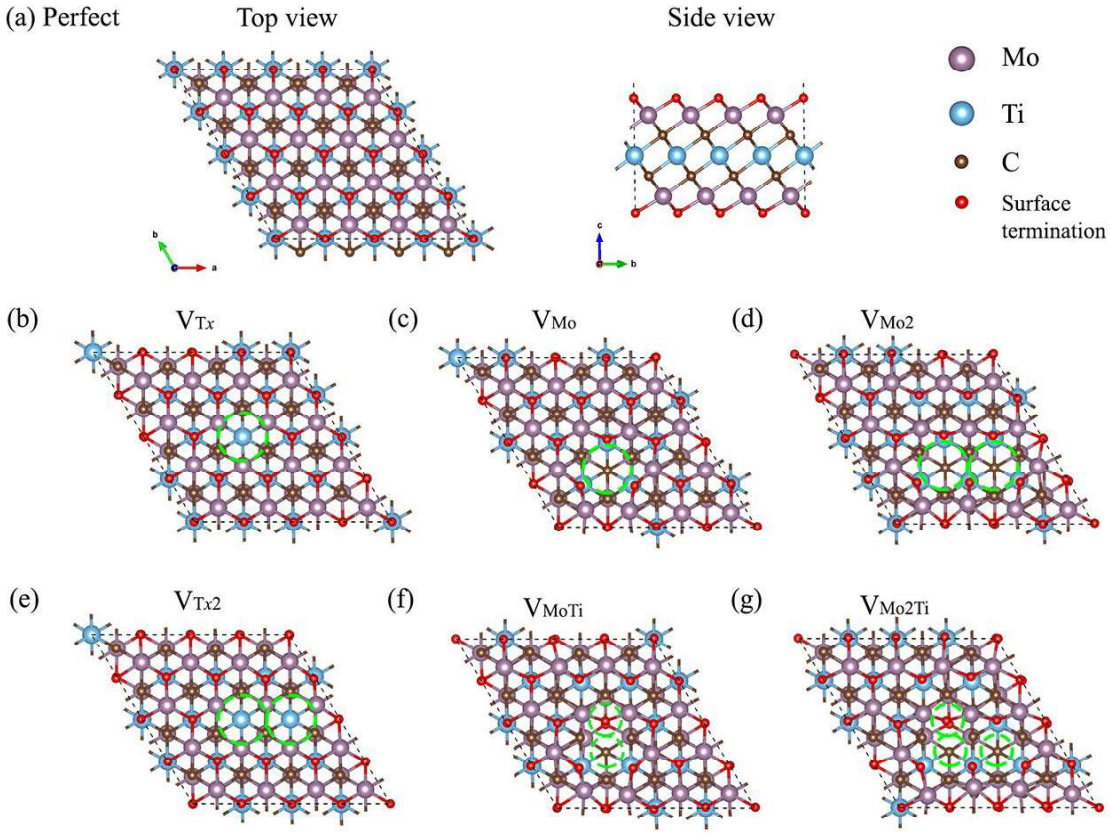

Fig. 1 Fully relaxed structural models of different types of defects considered in monolayer ordered $Mo_2TiC_2T_x$ (a) Top and side view of the perfect MXene. Top views of (b) V_{Tx}, (c) V_{Mo}, (d) V_{Mo2}, (e) V_{Tx2}, (f) V_{MoTi}, and (g) V_{Mo2Ti}.

In this study, we performed first-principles calculations based on density functional theory (DFT) to explore the effects of different types of defects on the structural stability, electronic behavior, and electrochemical properties of ordered $Mo_2TiC_2T_x$ (T = O, F, and OH). The formation of defects on the top and bottom molybdenum sublayers is more feasible because of the direct contact with the etchant solution, however, the presence of defects in the titanium layer is also possible that are inherited from the MAX phase. Moreover, the cluster-defects were observed within the same sublayer in $Ti_3C_2T_x$ MXene.[10] **Fig. 1** shows the optimized defect structures of seven different types of defects considered, including single T_x vacancy (V_{Tx}) and two adjacent T_x vacancies (V_{Tx2}) on both sides of the flake, single molybdenum vacancy (V_{Mo}), two adjacent molybdenum vacancies (V_{Mo2}) within the same sublayer, vacancy complex of single molybdenum and nearby one titanium (V_{MoTi}), vacancy complex of two adjacent molybdenum forming within the same sublayer and nearby one titanium (V_{Mo2Ti}), two

molybdenum vacancies forming within two different sublayers (V_{MoMo}). The top view of V_{MoMo} is the same as V_{Mo} and is not shown in **Fig. 1**. The structural stability of all types of defects is investigated through their formation energies. The electronic properties of these defected $Mo_2TiC_2T_x$ MXenes are also analyzed to highlight the influence of these effects on the conductance of MXene terminated with different functional groups. The effects of these defects on the electrochemical properties of MXene are also studied by evaluating CO_2 adsorption performance on $Mo_2TiC_2O_2$.

2 Computational methods

First-principles calculations based on density functional theory (DFT) are performed using Vienna *ab initio* Simulation Package (VASP).[26] We employed the generalized gradient approximation with the Perdue–Burke–Ernzerhof (PBE)[27] to describe the exchange and correlation of electrons. Projected augmented-wave (PAW)[28] potential is applied to take the interaction between ion-core and valence electrons into consideration and a plane wave basis set with a sufficient energy cutoff of 520 eV is employed to consider valence electrons. A 4×4×1 supercell is used to model 2D $Mo_2TiC_2T_x$ (T = F, O, and OH) MXene monolayers to provide at least 10 Å distance between the point defects. A large vacuum of at least 20 Å is used to avoid any undesirable interaction between an MXene sheet and its periodically repeated images along the *c*-axis. The Brillouin zone is sampled with a 5×5×1 Monkhorst-Pack[29] *k*-points for structural optimizations and with a 10×10×1 mesh for electronic structure analysis. The atomic positions and lattice constants are fully optimized using the conjugate gradient method. The geometries of the MXenes are relaxed until the forces acting on each atom become less than 0.001 eV/Å. The criterion for energy convergence is 10^{-6} eV/cell. The partial occupancies are determined using the Methfessel–Paxton smearing scheme with a smearing width of 0.1 eV.[30] We employed a spin-dependent GGA plus Hubbard U (GGA + U)[31] methodology to apply the correlation effects in transition metals of Mo and Ti with a value of U = 4 eV, which have been applied for $Mo_2TiC_2T_x$ MXenes[8] and extensively applied for their oxides.[32,33] We performed the spin-polarized DFT calculations with the antiferromagnetic (AFM) configurations predicted by Anasori et al.[8] for the $Mo_2TiC_2T_x$ MXenes chemically terminated by different terminations.

We calculated the formation energies of defects as $E_f = E_{MXene\_defect} - E_{MXene\_perfect} + \sum_i n_i\mu_i$, where

E_{MXene_defect} and $E_{MXene\_perfect}$ are the total energies of the MXene supercell with specific defects and related perfect structure without defect, respectively, n_i is the number of removed atoms, and μ_i is the chemical potential of the removed atom(s). Since it is not straightforward obtaining the exact value of μ_i, which is dependent on pressure and temperature,[34] we calculated E_f with the chemical potential between −2.0 to 0.0 eV.

The adsorption energy of the CO_2 molecule is calculated as $E_{ads} = E_{MXene+mol} - (E_{MXene} + E_{mol})$ by taking Van Der Waals (vdW) interactions into account by employing the dispersion-corrected DFT-D2 scheme,[35] which is essential for the accurate description of the interaction between CO_2 and a surface.[36–38] $E_{MXene+mol}$ is the total energy of the adsorbate−substrate system; E_{MXene} is the energy of the MXene monolayer; and E_{mol} is the energy of the isolated CO_2 molecule. We investigated the CO_2 adsorption on the MXene by placing the molecule close to different sites of the monolayer parallel and perpendicularly in different possible directions to find the most adsorption energy. The negative (positive) values of adsorption energy indicate an exothermic (endothermic) process.

3 Results and discussion

3.1 Formation energy of defects

We calculated the formation energy of different types of defects considered (see **Fig. 1**) in both non-terminated and terminated ordered MXene to better understanding the energetic costs of the formation of defects. We first evaluated these energies for a non-terminated Mo_2TiC_2 to gain more information about the feasibility of forming defects during the first step of exfoliation when the flakes are not terminated. Then, those energies are presented for terminated MXene with specific functional groups.

Our results for non-terminated MXene (**Fig. 2a**) indicate that the formation energies of V_{Mo} are lower than other types of defects, varying from 6.65 to 8.65 eV with the chemical potential between -2.0 to 0.0 eV. The formation of V_{Mo2} consumes approximately the same amount of energy as V_{MoMo} and almost twice as much energy as V_{Mo}, which indicates a linear relationship between the formation energy of defects and the number of V_{Mo}. This linear relationship was also found for titanium vacancy clusters up to six titanium vacancies from the outer sublayer of Ti_3C_2 MXene.[10] Moreover, V_{MoTi} and V_{Mo2Ti} detect formations are more energy consuming than other types of defects. The results show that defect

formations in titanium sublayer are energetically more difficult than within the outer molybdenum sublayers. Similar results confirming this was also reported by the study of Sang et al.,[10] where they calculated the formation energy of single titanium vacancy from the outer (2.85 eV) and inner (6.49 eV) sublayer of a 4×5×1 supercell of Ti_3C_2 MXene.

The effect of the surface functions on the calculated defect formation energies (**Figs. 2b**, **2c**, and **2d**) indicate relatively the same behavior as determined for pristine Mo_2TiC_2 MXene. The formation of V_{Mo}, V_{Mo2}, V_{MoTi}, V_{Mo2Ti}, and V_{MoMo} on the MXene terminated by oxygen (**Fig. 2c**) are more energy consuming than those for pristine non-terminated MXene (**Fig. 2a**), while the energetic costs of these defects on the MXenes terminated by fluorine and hydroxide (**Figs. 2b** and **2d**) are comparable with those on pristine MXene (**Fig. 2a**). The behavior is observed as oxygen gains more charge from transition metal atoms than fluorine and hydroxide and make the bond strength between transition metals and oxygen functional groups stronger.[9] The higher formation energy of titanium vacancy on $Ti_{n+1}C_nT_x$ (n = 1, 2) MXenes terminated by oxygen than that for pristine and –F and –OH terminated MXenes was also predicted.[10,25] Moreover, the calculated formation energies demonstrate that fluorine and hydroxide defect formations are comparable and are much more feasible than oxygen defect formation. It is worth mentioning that the formation of functional group atoms is considered on both sides of the flake because of the direct contact of the flakes with the etchant solution.

To further explore the effect of the replacement of the outer titanium layers in $Ti_3C_2T_x$ MXene by molybdenum layers on the defect formation energies, we compared our calculated formation energies of V_{Mo} on a 4×4×1 supercell of $Mo_2TiC_2T_x$ MXene with the calculated formation energies of V_{Ti} from the outer titanium sublayers of a 4×5×1 supercell of $Ti_3C_2T_x$ MXene.[10] We scaled linearly their calculated formation energies of V_{Ti} to provide the same vacancy concentration considered in our study since they predicted a linear relationship between the formation energies of V_{Ti} clusters with the number of V_{Ti}. The scaled formation energies of V_{Ti} in pristine Ti_3C_2 MXene (Ti_3C_2-V_{Ti}: 3.56 eV) and terminated $Ti_3C_2T_x$ MXenes ($Ti_3C_2F_2$-V_{Ti}: 4.53, $Ti_3C_2O_2$-V_{Ti}: 9.68, $Ti_3C_2(OH)_2$-V_{Ti}: 4.34) indicate that the replacement of the outer titanium layers in $Ti_3C_2T_x$ MXene by molybdenum layers make the formation of defects more difficult in non-terminated Mo_2TiC_2 MXene and terminated MXenes by

fluorine and hydroxide; however, the formation of defects in MXene terminated by oxygen functional groups are comparable. This is because of the fact that Mo-Mo bonds are stronger than Ti-Ti bonds.[39] Thus, based on our study, the energetic costs of the formation of defects become higher by manipulating the outer titanium layers in $Ti_3C_2T_x$ MXene by molybdenum layers because of the intrinsic bond strengths in these two MXene systems and V_{Mo} is the most probable defect to form during the synthesis of MXene monolayers.

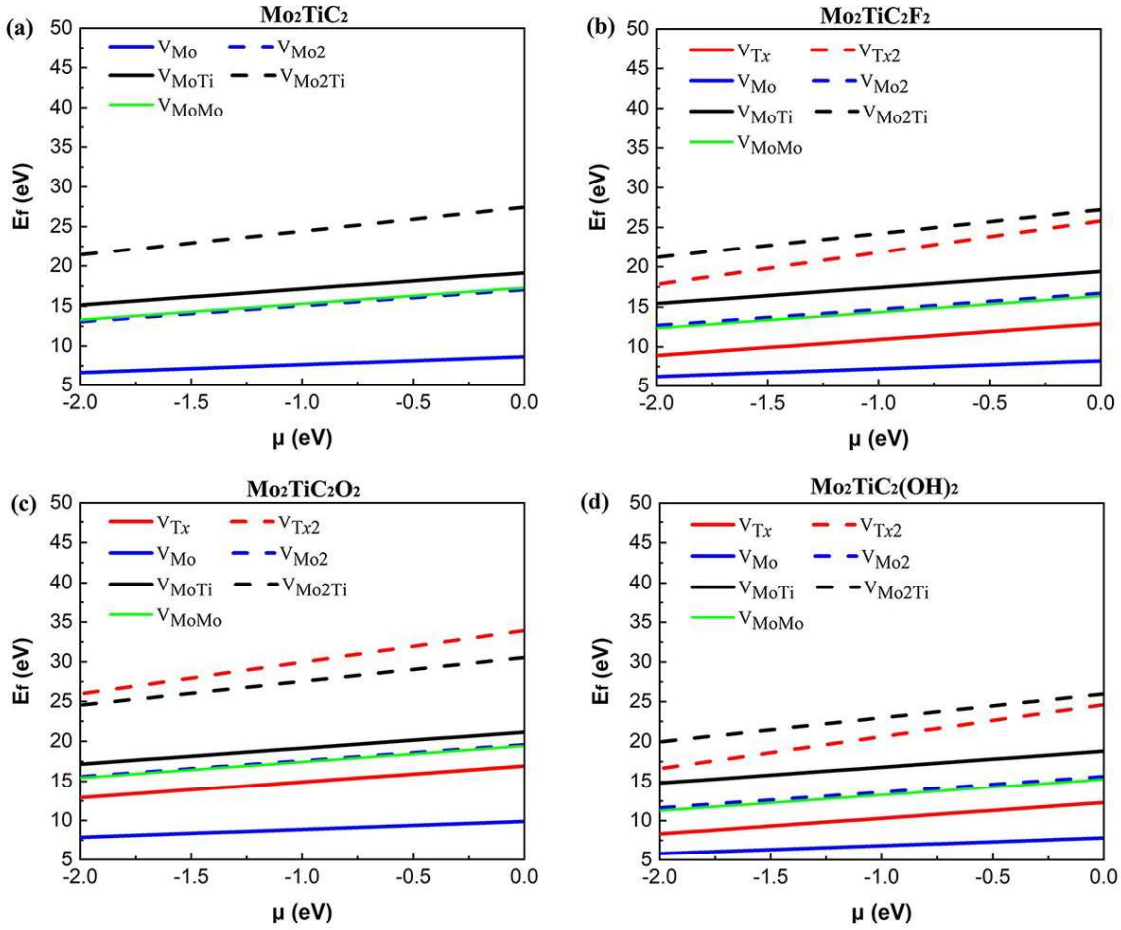

Fig. 2 Formation energies of all types of defects as a function of the chemical potential of the removed atom(s) in the range of -2 eV < μ < 0 e in (a) Mo_2TiC_2, (b) $Mo_2TiC_2F_2$, (c) $Mo_2TiC_2O_2$, (d) $Mo_2TiC_2(OH)_2$.

3.2 Electronic properties

Before evaluating the electronic properties of defected $Mo_2TiC_2T_x$ Mxenes, we present the electronic properties of perfect $Mo_2TiC_2T_x$ Mxenes with different terminations. The total densities of states (DOS) of perfect MXenes are displayed in **Fig. 3**. Similar to all predicted pristine mono-M element MXenes (M is a transition metal) which are metallic,[9] the results indicate that the pristine ordered Mo_2TiC_2

MXene is also metallic (**Fig. 3a**). It was predicted that some of the mono-M element MXenes with surface terminations could exhibit semiconducting behavior depending upon the participating components and surface terminations.[9] Here, we consider a specific surface termination (e.g., pure -F, -O or -OH) and our results show that ordered $Mo_2TiC_2T_x$ Mxenes terminated by F and OH become semiconducting (**Figs. 3b** and **3d**) and the band-gap of OH-terminated MXene is smaller than that of F-terminated MXene, while O-terminated MXene exhibit metallic behavior (**Fig. 3c**). Our results are in reasonable agreement with an earlier study by Anasori et al.[8], where they also investigated the electronic structure of MXene with mixed terminations since it was observed from EDX analysis that the synthesized surface has a mixture of -F, -O, and -OH terminations. Their results indicated that the synthesized $Mo_2TiC_2T_x$ MXene has a semiconducting behavior, except for the MXene terminated by high concentrations of oxygen.

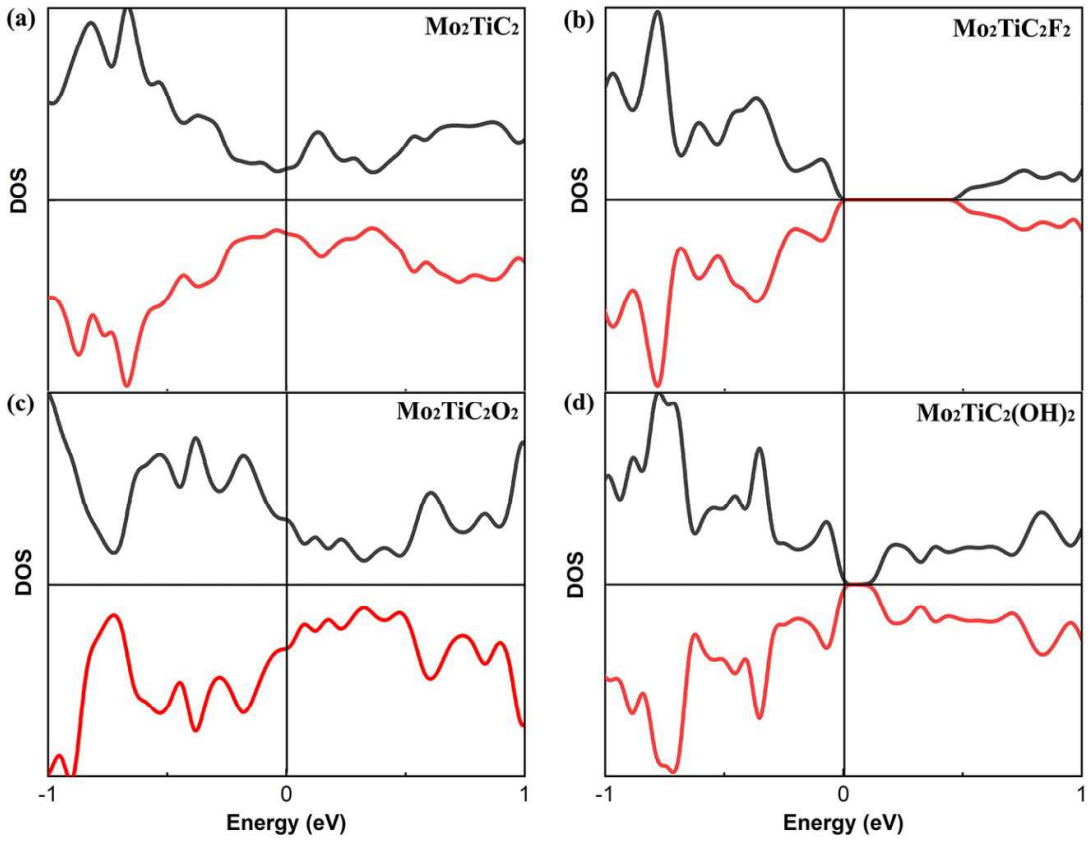

Fig. 3 Calculated the total density of states (DOS) of perfect MXene. (a) Pristine MXene, (b) $Mo_2TiC_2F_2$, (c) $MoTiC_2O_2$, and (d) $Mo_2TiC_2(OH)_2$. Black and red lines show spin-up and –down states, respectively.

The effect of different types of defects on the electronic properties of non-terminated and terminated ordered MXene is evaluated. Our calculated results of total DOS of non-terminated MXene (**Fig. S1**; **Supporting Information**) indicate that defective Mo_2TiC_2 MXene is still metallic. **Fig. 4** presents the DOS of different type of defected MXenes under investigation, while for all different surface terminated Mxenes (F, O and OH), it is very clear that detects V_{Tx} make these MXenes again to be metallic as we can observe states due to vacancies crossing fermi energy levels in these structures (**Fig. 4a**, **4e,** and **4i**). For V_{MO} and V_{MoMo} vacancies, we do not observe any significant change in the electronic DOS of the structures, while for F and OH terminations, Mxenes are semiconducting, while for O terminations the structure retains their metallic nature. From other defected Mxenes, we can conclude that there are very minor changes in the electronic states, making structures to be more semiconducting due to shifting in bands away from a Fermi energy level.

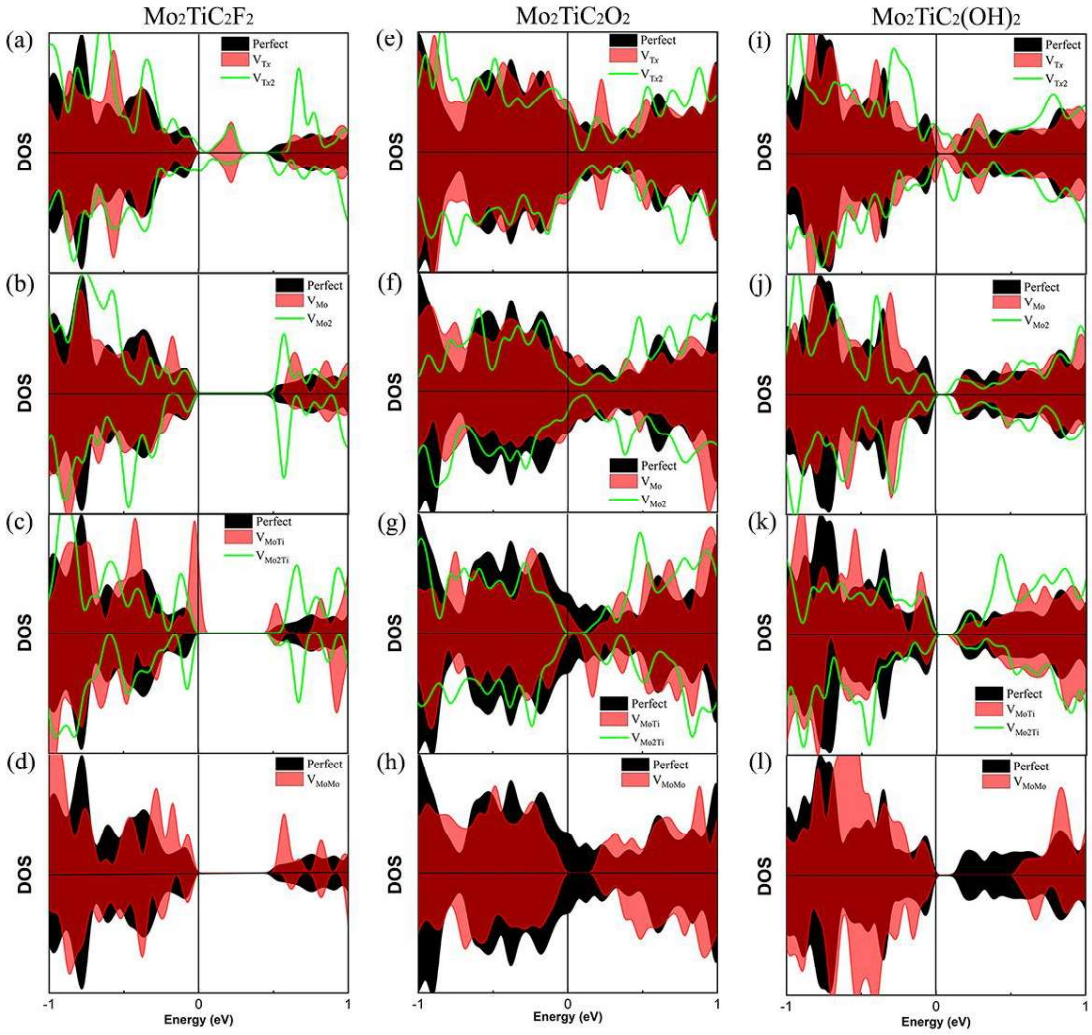

Fig. 4 Effect of different types of defects on the DOS of MXene with different terminations. (a)–(d) $Mo_2TiC_2F_2$, (e)–(h) $Mo_2TiC_2O_2$, and (i)–(l) $Mo_2TiC_2(OH)_2$. The type of defect is shown on the different panels.

3.3 CO_2 adsorption on $Mo_2TiC_2O_2$ defects

The interactions of different molecules with the defective structures such as TiO_2,[40] graphene and silicene,[41] BCN,[42] and MoS_2[43–47] demonstrated that the molecular adsorption on the surfaces could be enhanced in the presence of defects. In this section, the influence of considered defects on the reactivity and electrochemical transport properties of $Mo_2TiC_2T_x$ MXene are investigated by modeling the interaction of a CO_2 molecule on the monolayer. Here, we consider only the MXene terminated by oxygen surface functions. We first, evaluate the capability of a 3×3×1 supercell of the clean $Mo_2TiC_2O_2$ MXene for the CO_2 adsorption. Then, we discuss the reactivity of defected $Mo_2TiC_2O_2$ MXenes with a CO_2 molecule.

Our calculated results indicate that the CO_2 molecule is physisorbed on the clean $Mo_2TiC_2O_2$ MXene, with nonspontaneous reaction energy of 0.21 eV (see **Fig. 5a**). The carbon atom of CO_2 interacts with the oxygen surface functions and the molecule is placed at a distance of 2.89 Å while it is not significantly tilted. Moreover, a comparative nonspontaneous Gibbs free reaction energy (at 298.15 K) of 0.23 eV for the physisorption of CO_2 molecule on $Mo_3C_2O_2$ MXene was calculated.[48] Thus, we can realize that Mo-containing MXenes are weakly reactive for CO_2 capture.

We further evaluated the proficiency of defected $Mo_2TiC_2O_2$ MXenes in the CO_2 adsorption. Before that, we analyzed the electron localization function (ELF) over the surfaces, which provides a qualitative understanding of the empirical concept of electron localization and the behavior of the electrons over the defected surfaces, as shown in **Fig. 6**. The calculated ELFs for non-terminated MXene and MXenes terminated by fluorine and hydroxide are shown in **Figs. S2**, **S3**, and **S4** (**Supporting Information**), respectively. ELF is defined in the range between 0 and 1, where the upper limit of ELF = 1 exhibits the perfect localization and ELF = 0.5 corresponds to the uniform electron gas. Here, we showed the ELFs in the range between 0 and 0.5 since the perfect localization was not detected over the surfaces. As it is shown in **Fig. 6**, electrons are generally localized on the surface functional groups over the MXene. In the case of V_{Tx} and V_{Tx2}, electrons are completely delocalized on the place of the removed oxygen atom(s) and are freely moved to other oxygen atoms on the surface. However, in other types of defects, electrons are partially delocalized on the oxygen atoms close to the removed atoms and are moved to other places. Based on the ELF analysis, we placed the CO_2 molecule close to different sites of the monolayer, in which electrons are more localized, parallel and perpendicularly in different possible directions to find the most adsorption energy in defective MXenes.

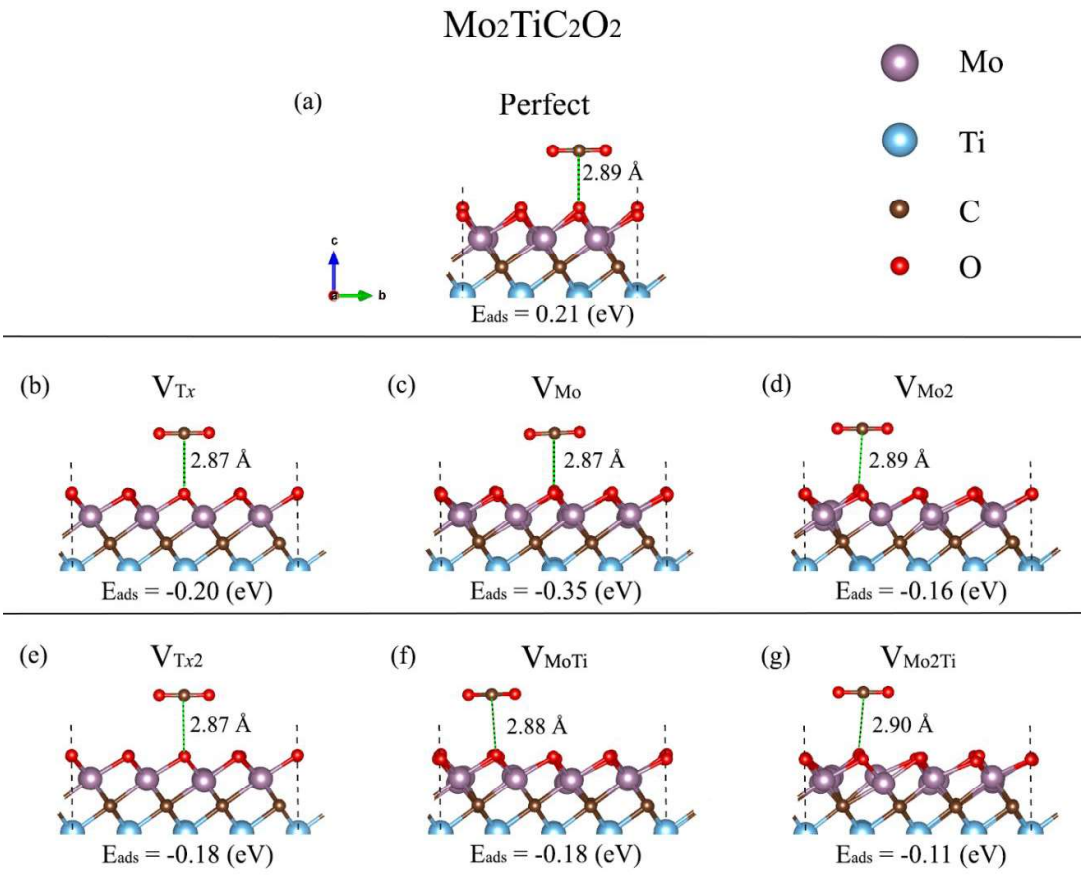

Fig. 5 Relaxed adsorption configurations of CO_2 molecule on perfect and defected $Mo_2TiC_2O_2$ MXene. (a) Perfect MXene, (b) MXene-V_{Tx}, (c) MXene-V_{Mo}, (d) MXene-V_{MO2}, (e) MXene-V_{Tx2}, (f) MXene-V_{MoTi}, and (g) MXene-V_{Mo2Ti}.

Our calculated adsorption energies (**Fig. 5**) imply that the molecule spontaneously adsorbs on defected surfaces with the adsorption energies between -0.11 and -0.35 eV, hence indicating that the molecule is trapped in the defect. The molecule is placed at distances between 2.87 and 2.90 Å and not considerably tilted, relatively similar to the case of perfect MXene. The adsorption energies on the defected surfaces including V_{Tx} and V_{Tx2} are comparative (-0.20 and -0.18 eV, respectively). The molecule is highly attracted by the defect formed by a single Mo atom with spontaneous reaction energy of -0.35 eV, while our results show spontaneous reaction energy of -0.16 eV for MXene-V_{Mo2}. Moreover, the results indicate that Ti vacancy decreases the proficiency of MXene-V_{Mo} and MXene-V_{Mo2} in the CO_2 adsorption from -0.35 to -0.18 eV in MXene-V_{Mo} and from -0.16 to -0.11 eV in MXene-V_{Mo2}. We also performed Bader charge analyses of the perfect and defected MXene-CO_2 systems to quantify the electron transfer from the MXenes to the CO_2 molecule, but we observed that the charge transfer to the

CO_2 molecule is quite negligible since the molecule is not chemisorbed on the surfaces. The electron density difference isosurface plot for the case of the MXene-V_{Tx} surface, as an example, is shown in **Fig. S5** (**Supporting Information**).

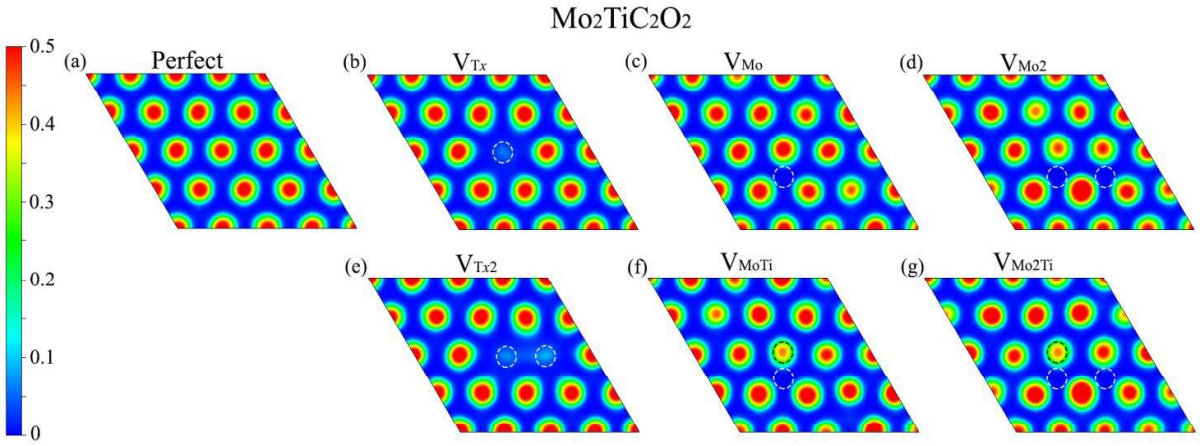

Fig. 6 Electron localization function (ELF) on the plane perpendicular to the *c*-axis at the close distance on top of surface terminations of the defected $Mo_2TiC_2O_2$ MXenes. Dash circle lines highlight the place of the removed atoms.

4 Conclusion

In the present work, we have investigated atomic defects in ordered $Mo_2TiC_2T_x$ terminated with specific surface functions of fluorine, oxygen or hydroxide. Different atomic vacancy detects in top and sublayer including surface atom vacancies have been studied. Through detect formation energies calculations, we conclude that defects are dependent on the surface terminations, where the O-terminated MXenes demand more energy than F- and OH-terminated MXenes, also the defect formation is more feasible in outer molybdenum layers than inner titanium layer. While, DOS calculations indicate that there are minor changes in the electronic states with a shift in states away from the Fermi energy level, making the system more semiconducting.

Our vacancy mediated activation of CO_2 molecule indicates the potential catalytic properties of the $Mo_2TiC_2T_x$ MXenes and results indicate that CO_2 molecule can be activated by forming the defects in the monolayer. While the CO_2 molecule adsorbs on the perfect O-terminated MXene through a nonspontaneous and endothermic process, defect formations on the monolayer lead to the direct CO_2 interactions with the surfaces through a spontaneous and exothermic process that is crucial to its capture. Our study exhibit that the defect formations on the monolayer cannot activate the CO_2 molecule since

the bond angle ∠O-C-O is not considerable changed. Our study unveils a way to the possibility of enhancing the catalytic properties of $Mo_2TiC_2T_x$ MXenes by the forming of specific defects in the monolayer.

Conflicts of interest

There are no conflicts to declare.

Acknowledgments

The authors would like to acknowledge and greatly appreciate the financial support from VISTA which is a basic research program in collaboration between the Norwegian Academy of Science and Letters, and Equinor. The authors would also like to thank the Department of Mechanical and Industrial Engineering at the Norwegian University of Science and Technology (NTNU). The authors also acknowledge generous grants of high-performance computer time from both Vilje and UNINETT Sigma. One of the authors (AKM) acknowledges the SEED grant from the University of Petroleum and Energy Studies (UPES).

References

1 B. Anasori, M. R. Lukatskaya and Y. Gogotsi, 2D metal carbides and nitrides (MXenes) for energy storage, *Nat. Rev. Mater.*, 2017, **2**, 16098.

2 M. Zhao, M. Torelli, C. E. Ren, M. Ghidiu, Z. Ling, B. Anasori, M. W. Barsoum and Y. Gogotsi, 2D titanium carbide and transition metal oxides hybrid electrodes for Li-ion storage, *Nano Energy*, 2016, **30**, 603–613.

3 M. Naguib, J. Halim, J. Lu, K. M. Cook, L. Hultman, Y. Gogotsi and M. W. Barsoum, New two-dimensional niobium and vanadium carbides as promising materials for li-ion batteries, *J. Am. Chem. Soc.*, 2013, **135**, 15966–15969.

4 Y. Peng, B. Akuzum, N. Kurra, M. Zhao, M. Alhabeb, B. Anasori, E. C. Kumbur, H. N. Alshareef, M. Ger and Y. Gogotsi, All-MXene (2D titanium carbide) solid-state microsupercapacitors for on-chip energy storage, *Energy Environ. Sci.*, 2016, **9**, 2847–2854.

5 G. Fan, X. Li, Y. Ma, Y. Zhang, J. Wu, B. Xu, T. Sun, D. Gao and J. Bi, Magnetic, recyclable PtyCo1−y/Ti3C2X2 (X = O, F) catalyst: a facile synthesis and enhanced catalytic activity for hydrogen generation from the hydrolysis of ammonia borane, *New J. Chem.*, 2017, **41**, 2793–2799.

6 B. Anasori, Y. Xie, M. Beidaghi, J. Lu, B. C. Hosler, L. Hultman, P. R. C. Kent, Y. Gogotsi and M. W. Barsoum, Two-Dimensional, Ordered, Double Transition Metals Carbides (MXenes), *ACS Nano*, 2015, **9**, 9507–9516.

7 M. Naguib, M. Kurtoglu, V. Presser, J. Lu, J. Niu, M. Heon, L. Hultman, Y. Gogotsi and M. W. Barsoum, Two-Dimensional Nanocrystals Produced by Exfoliation of Ti3AlC2, *Adv. Mater.*, 2011, **23**, 4248–4253.

8 B. Anasori, C. Shi, E. J. Moon, Y. Xie, C. A. Voigt, P. R. C. Kent, de S. J. May, S. J. L. Billinge, M. W. Barsoum and Y. Gogotsi, Control of electronic properties of 2D carbides (MXenes) by manipulating their transition metal layers, *Nanoscale Horizons*, 2016, **1**, 227–234.

9 M. Khazaei, A. Ranjbar, M. Arai and S. Yunoki, Electronic properties and applications of MXenes: a theoretical review, *J. Mater. Chem. C*, 2017, **5**, 2488–2503.

10 X. Sang, Y. Xie, M. Lin, M. Alhabeb, K. L. Van Aken, Y. Gogotsi, P. R. C. Kent, K. Xiao and R. R. Unocic, Atomic Defects in Monolayer Titanium Carbide, *ACS Nano*, 2016, **10**, 9193–9200.

11 L. H. Karlsson, J. Birch, J. Halim, M. W. Barsoum and P. O. Å. Persson, Atomically Resolved Structural and Chemical Investigation of Single MXene Sheets, *Nano Lett.*, 2015, **15**, 4955–4960.

12 J. Halim, S. Kota, M. R. Lukatskaya, M. Naguib, M. Zhao, E. J. Moon, J. Pitock, J. Nanda, S. J. May, Y. Gogotsi and M. W. Barsoum, Synthesis and Characterization of 2D Molybdenum

Carbide (MXene), *Adv. Funct. Mater.*, 2016, **2**, 3118–3127.

13 A. Lipatov, M. Alhabeb, M. R. Lukatskaya, A. Boson, Y. Gogotsi and A. Sinitskii, Effect of synthesis on quality, electronic properties and environmental stability of individual monolayer Ti3C2 MXene flakes, *Adv. Electron. Mater.*, 2016, **2**, 1600255.

14 L. Vicarelli, S. J. Heerema, C. Dekker and H. W. Zandbergen, Controlling Defects in Graphene for Optimizing the Electrical Properties of Graphene Nanodevices, *ACS Nano*, 2015, **9**, 3428–3435.

15 G. López-polín, C. Gómez-navarro, V. Parente, M. I. Katsnelson, F. Pérez-murano and J. Gómez-herrero, Increasing the elastic modulus of graphene by controlled defect creation, *Nat. Phys.*, 2015, **11**, 26.

16 F. Banhart, J. Kotakoski and A. V Krasheninnikov, Structural Defects in Graphene, *ACS Nano*, 2011, **5**, 26–41.

17 D. Wong, J. V. Jr, L. Ju, J. Lee, S. Kahn, H. Tsai, C. Germany, T. Taniguchi, K. Watanabe, A. Zettl, F. Wang and M. F. Crommie, Characterization and manipulation of individual defects in insulating hexagonal boron nitride using scanning tunnelling microscopy, *Nat. Nanotechnol.*, 2015, **10**, 949–953.

18 Y. Liu, X. Zou and B. I. Yakobson, Dislocations and Grain Boundaries in Two-Dimensional Boron Nitride, *ACS Nano*, 2012, **6**, 7053–7058.

19 R. Bourrellier, S. Meuret, A. Tararan, O. Ste, M. Kociak, L. H. G. Tizei and A. Zobelli, Bright UV Single Photon Emission at Point Defects in h-BN, *Nano Lett.*, 2016, **16**, 4317–4321.

20 W. Zhou, X. Zou, S. Najmaei, Z. Liu, Y. Shi, J. Kong and J. Lou, Intrinsic Structural Defects in Monolayer Molybdenum Disulfide, *Nano Lett.*, 2013, **13**, 2615– 2622.

21 M. Amani, D. Lien, D. Kiriya, J. Xiao, A. Azcatl, J. Noh, S. R. Madhvapathy, R. Addou, M. Dubey, K. Cho, R. M. Wallace, S. Lee, J. He, X. Zhang, E. Yablonovitch and A. Javey, Near-unity photoluminescence quantum yield in MoS2, *Sci. (Washington, DC, U. S.)*, 2015, **350**, 1065–1068.

22 Y. Wei, J. Wu, H. Yin, X. Shi, R. Yang and M. Dresselhaus, The nature of strength enhancement and weakening by pentagon – heptagon defects in graphene, *Nat. Mater.*, 2012, **11**, 759–763.

23 O. V Yazyev and S. G. Louie, Electronic transport in polycrystalline graphene, *Nat. Mater.*, 2010, **9**, 806–809.

24 T. Hu, X. Wang and Xiaohui Wang, Carbon vacancies in Ti2CT2 MXenes: defects or a new opportunity?, *Phys. Chem. Chem. Phys.*, 2017, **19**, 31773–31780.

25 A. Bandyopadhyay, D. Ghosh and S. K. Pati, Effects of point defects on the magnetoelectronic structures of MXenes from first principles, *Phys. Chem. Chem. Phys.*, 2018, **20**, 4012–4019.

26 G. Kresse and J. Furthmiiller, Efficiency of ab-initio total energy calculations for metals and semiconductors using a plane-wave basis set, *Comput. Mater. Sci.*, 1996, **6**, 15–50.

27 J. P. Perdew, K. Burke and M. Ernzerhof, Physical review letters, *Phys. Rev. Lett.*, 1996, 3865–3868.

28 G. Kresse and D. Joubert, From ultrasoft pseudopotentials to the projector augmented-wave method, *Phys. Rev. B*, 1999, **59**, 11–19.

29 H. J. Monkhorst and J. D. Pack, Special points for Brillonin-zone integrations, *Phys. Rev. B Solid State*, 1976, 5188–5192.

30 M. Methfessel and A. T. Paxton, High-precision sampling for Brillouin-zone integration in metals, *Phys. Rev. B*, 1989, **40**, 3616–3621.

31 S. L. Dudarev, G. A. Botton, S. Y. Savrasov, C. J. Humphreys and A. P. Sutton, Electron-energy-loss spectra and the structural stability of nickel oxide:, *Phys. Rev. B*, 1998, **57**, 1505–1509.

32 M. Nolan, S. D. Elliott, J. S. Mulley, R. A. Bennett and M. Basham, Electronic structure of point defects in controlled self-doping of the TiO2 (110) surface: Combined photoemission spectroscopy and density functional theory study, *Phys. Rev. B*, 2008, **77**, 235424.

33 G. Hautier, S. P. Ong, A. Jain, C. J. Moore and G. Ceder, Accuracy of density functional theory in predicting formation energies of ternary oxides from binary oxides and its implication on phase stability, *Phys. Rev. B - Condens. Matter Mater. Phys.*, 2012, **85**, 155208.

34 W.-X. Li, C. Stampfl and M. Scheffler, Insights into the function of silver as an oxidation catalyst by ab initio atomistic thermodynamics, *Phys. Rev. B*, 2003, **68**, 165412.

35 S. Grimme, Semiempirical GGA-Type Density Functional Constructed with a Long-Range Dispersion Correction, *J. Comput. Chem.*, 2006, **27**, 1787–1799.

36 R. Khaledialidusti, A. K. Mishra and A. Barnoush, CO2 Adsorption and Activation on the (110) Chalcopyrite Surfaces: A Dispersion-Corrected DFT + U Study, *ACS Omega*, , DOI:10.1021/acsomega.9b01988.

37 R. Khaledialidusti, A. K. Mishra and A. Barnoush, Rheological properties of super critical CO2 with CuO: Multi-scale computational modeling, *J. Chem. Phys.*, 2018, **149**, 224702.

38 A. K. Mishra, A. Roldan and N. H. De Leeuw, CuO Surfaces and CO2 Activation: A Dispersion-Corrected DFT+ U Study, *J. Phys. Chem. C*, 2016, **120**, 2198-2214.

39 M. Khazaei, A. Ranjbar, D. Bogdanovski and R. Dronskowski, Insights into exfoliation possibility of MAX phases to MXenes, *Phys. Chem. Chem. Phys.*, 2018, **20**, 8579–8592.

40 O. Bikondoa, C. L. Pang, R. Ithnin, C. A. Muryn, H. Onishi and G. Thornton, Direct visualization of defect-mediated dissociation of water on TiO2 (110), *Nat. Mater.*, 2006, **5**, 189–192.

41 H. H. Gürel, V. O. O. Zçelik and S. Ciraci, Dissociative Adsorption of Molecules on Graphene and Silicene, *J. Phys. Chem. C*, 2014, **118**, 27574–27582.

42 N. Kumar, K. Moses, K. Pramoda, S. N. Shirodkar, A. K. Mishra, U. V. Waghmare, A. Sundaresana and C. N. R. Rao, Borocarbonitrides, BxCyNz, *J. Mater. Chem. A*, 2013, 5806–5821.

43 S. Cho, S. J. Kim, Y. Lee, J. Kim, W. Jung, H. Yoo, J. Kim, H. Jung, B. Engineering, A. Technology, A. Development and D. Development, Highly Enhanced Gas Adsorption Properties in Vertically Aligned MoS2 Layers, *ACS Nano*, 2015, **9**, 9314–9321.

44 L. Qi, Y. Wang, L. Shen and Y. Wu, Chemisorption-induced n-doping of MoS2 by oxygen, *Appl. Phys. Lett.*, 2016, **1089**, 063103.

45 B. Akdim, R. Pachter and S. Mou, Theoretical analysis of the combined effects of sulfur vacancies and analyte adsorption on the electronic properties of single- layer MoS2, *Nanotechnology*, 2016, **27**, 185701.

46 H. Li, M. Huang and G. Cao, Markedly different adsorption behaviors of gas molecules on defective monolayer MoS2: a first-principles study, *Phys. Chem. Chem. Phys.*, 2016, **18**, 15110–15117.

47 C. Gonzalez, B. Biel and Y. Dappe, Adsorption of small inorganic molecules on a defective MoS2 monolayer, *Phys. Chem. Chem. Phys.*, 2017, **19**, 9485.

48 N. Li, X. Chen, W. Ong, D. R. Macfarlane, X. Zhao, A. K. Cheetham and C. Sun, Understanding of Electrochemical Mechanisms for CO2 Capture and Conversion into Hydrocarbon Fuels in Transition-Metal Carbides (MXenes), *ACS Nano*, 2017, **11**, 10825–10833.

Atomic defects in monolayer ordered double transition metals carbide ($Mo_2TiC_2T_x$) MXene and CO_2 Activation

Rasoul Khaledialidusti,[*a] Abhishek Kumar Mishra,[b] Afrooz Barnoush[a,c]

[a]Department of Mechanical and Industrial Engineering, Norwegian University of Science and Technology (NTNU), 7491 Trondheim, Norway. E-mail: rasoul.khaledialidusti@ntnu.no

[b] Department of Physics, School of Engineering, University of Petroleum and Energy Studies, Bidholi via Premnagar, Dehradun 248007, INDIA.

[c]Curtin Corrosion Centre, WASM-MECE, Curtin University, Australia.

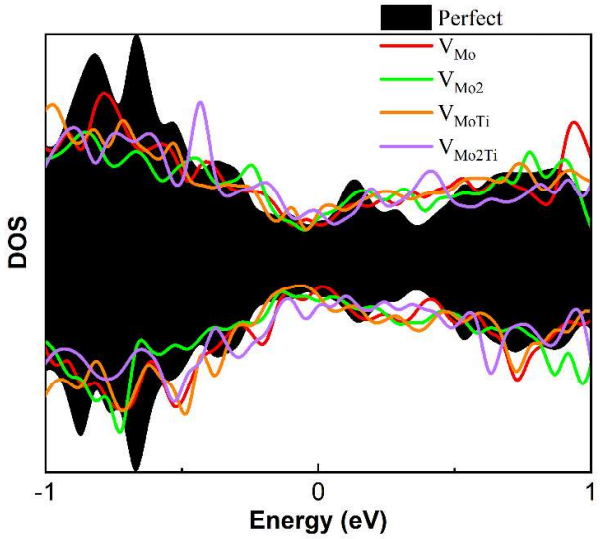

Fig. S1 Calculated total density of states (DOS) of perfect and defected Mo_2TiC_2 MXene.

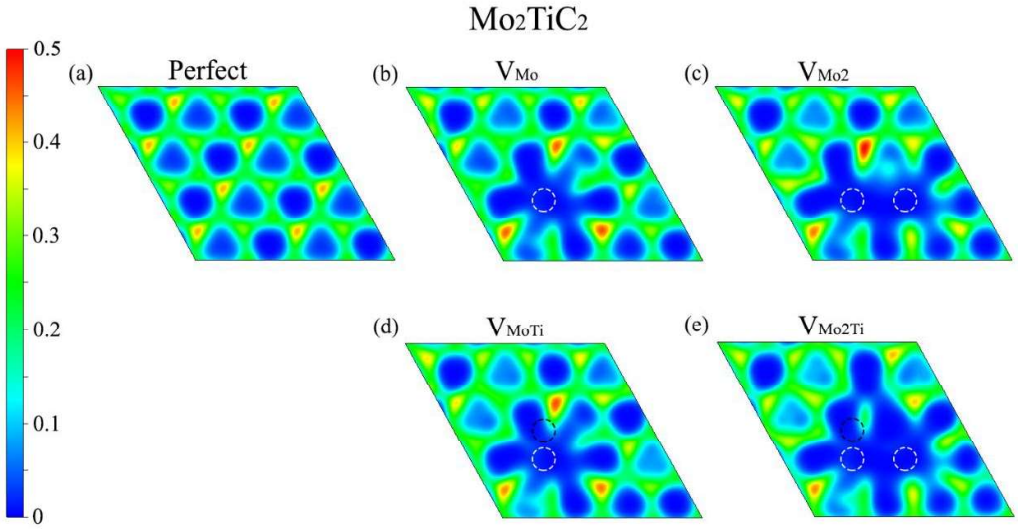

Fig. S2 Electron localization function (ELF) on the plane perpendicular to the *c*-axis at the close distance on top of surface terminations of the defected Mo_2TiC_2 MXenes. Dash circle lines highlight the place of the removed atoms.

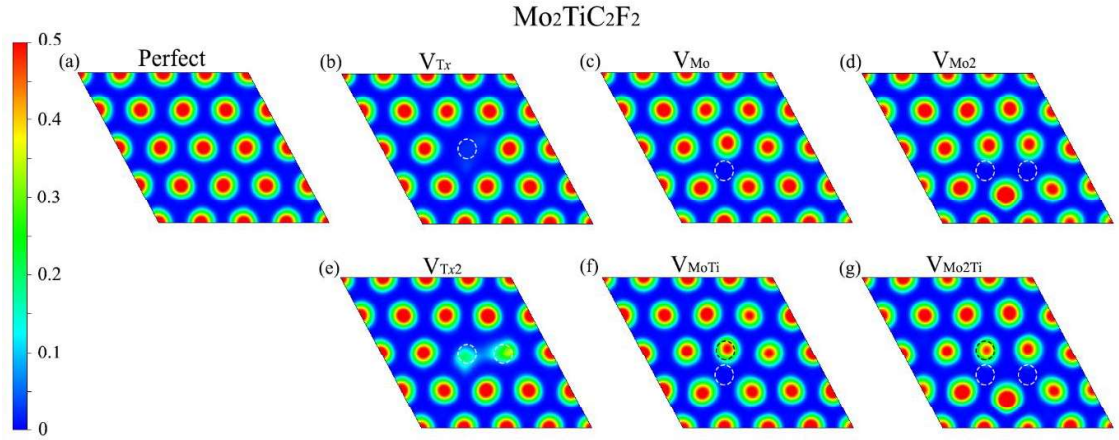

Fig. S3 Electron localization function (ELF) on the plane perpendicular to the *c*-axis at the close distance on top of surface terminations of the defected $Mo_2TiC_2F_2$ MXenes. Dash circle lines highlight the place of the removed atoms.

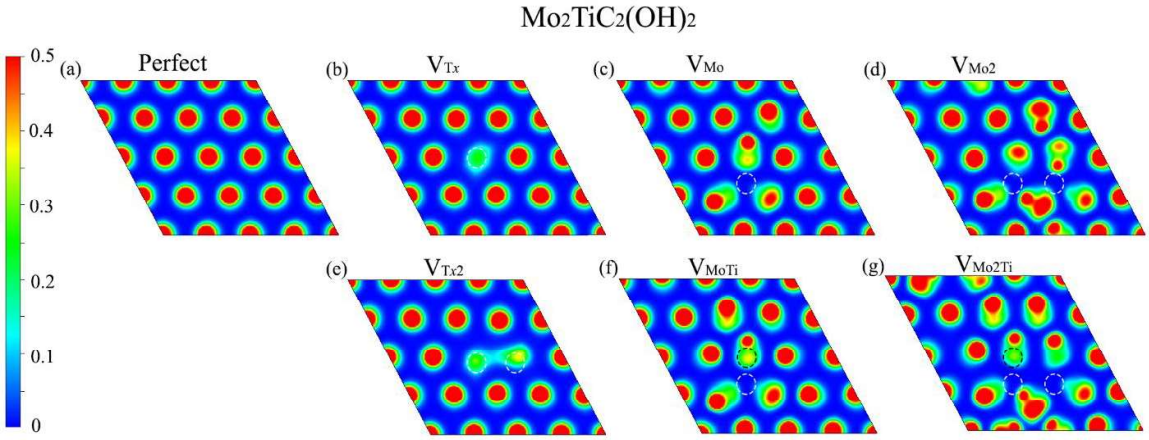

Fig. S4 Electron localization function (ELF) on the plane perpendicular to the *c*-axis at the close distance on top of surface terminations of the defected $Mo_2TiC_2(OH)_2$ MXenes. Dash circle lines highlight the place of the removed atoms.

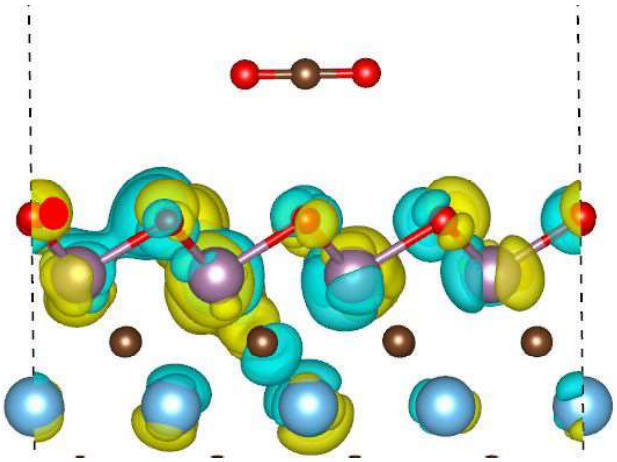

Fig. S5 Electronic density difference plot of CO_2 adsorption structures on MXene-V_{Tx} surface, showing no charge transfer in the regions between the CO_2 and the surface atoms since the molecule is not chemisorbed.